We are IntechOpen,
the world's leading publisher of
Open Access books
Built by scientists, for scientists

5,600
Open access books available

137,000
International authors and editors

170M
Downloads

Our authors are among the

154
Countries delivered to

TOP 1%
most cited scientists

12.2%
Contributors from top 500 universities

Interested in publishing with us?
Contact book.department@intechopen.com

Numbers displayed above are based on latest data collected.
For more information visit www.intechopen.com

Chapter

Analysis of Heat Transfer in Non-Coaxial Rotation of Newtonian Carbon Nanofluid Flow with Magnetohydrodynamics and Porosity Effects

Wan Nura'in Nabilah Noranuar,
Ahmad Qushairi Mohamad, Sharidan Shafie, Ilyas Khan,
Mohd Rijal Ilias and Lim Yeou Jiann

Abstract

The study analyzed the heat transfer of water-based carbon nanotubes in non-coaxial rotation flow affected by magnetohydrodynamics and porosity. Two types of CNTs have been considered; single-walled carbon nanotubes (SWCNTs) and multi-walled carbon nanotubes (MWCNTs). Partial differential equations are used to model the problem subjected to the initial and moving boundary conditions. Employing dimensionless variables transformed the system of equations into ordinary differential equations form. The resulting dimensionless equations are analytically solved for the closed form of temperature and velocity distributions. The obtained solutions are expressed in terms of a complementary function error. The impacts of the embedded parameters are graphically plotted in different graphs and are discussed in detail. The Nusselt number and skin friction are also evaluated. The temperature and velocity profiles have been determined to meet the initial and boundary conditions. An augment in the CNTs' volume fraction increases both temperature and velocity of the nanofluid as well as enhances the rate of heat transport. SWCNTs provides high values of Nusselt number compared to MWCNTs. For verification, a comparison between the present solutions and a past study is conducted and achieved excellent agreement.

Keywords: Nanofluids, Carbon nanotubes, Newtonian fluid, Magnetohydrodynamics, Heat transfer

1. Introduction

The growing demand in manufacturing has led to a significant process of heat energy transfer in industry applications such as nuclear reactors, heat exchangers, radiators in automobiles, solar water heaters, refrigeration units and the electronic cooling devices. Enhancing the heating and cooling processes in industries will save

energy, reduce the processing time, enhances thermal rate and increase the equipment's lifespan. Sivashanmugam [1] found that nanofluid emergence has improved heat transfer capabilities for processes in industries. Choi and Eastman [2] established the nanofluid by synthesizing nanoparticles in the conventional base fluid. To be specific, nanofluid is created by suspending nano-sized particles with commonly less than 100 nm into the ordinary fluids such as ethylene glycol, propylene glycol, water and oils [3]. Various materials from different groups can be used as the nanoparticles such as Al_2O_3 and CuO from metalic oxide, Cu, Ag, Au from metals, SiC and TiC from carbide ceramics, as well as TiO_3 from semiconductors [4]. In addition, immersion of nanoparticles is a new way of enhancing thermal conductivity of ordinary fluids which directly improves their ability in heat transportation [5]. In line with nanofluid's contribution in many crucial applications, a number of research has been carried out to discover the impacts of various nanofluid suspension on the flow features and heat transfer with several effects including Sulochana et al. [6] considering CuO-water and TiO-water, Sandeep and Reddy [7] using Cu-water, and Abbas and Magdy [8] choosing Al_2O_3-water as their nanofluid.

Magnetohydrodynamics (MHD) is known as the resultant effect due to mutual interaction of magnetic field and moving electrical conducting fluid. Their great applications such as power generation system, MHD energy conversion, pumps, motors, solar collectors have drawn significant attention of several researcher for MHD nanofluid in convective boundary layer flow [9]. Benos and Sarris [10] studied the impacts of MHD flow of nanofluid in a horizontal cavity. Hussanan et al. [11] analyzed the transportation of mass and heat for MHD nanofluid flow restricted to an accelerated plate in a porous media. In this study, water-based oxide and non-oxide had been considered as the nanofluids. Prasad et al. [12] performed similar work as [11] concerning the radiative flow of nanofluid over a vertical moving plate. Anwar et al. [13] conducted the MHD nanofluid flow in a porous material with heat source/sink and radiation effects. Cao et al. [14] analyzed the heat transfer and flow regimes for a Maxwell nanofluid under MHD effect. While, Ramzan et al. [15] investigated for a radiative Jeffery nanofluid and Khan et al. [16] carried out for a Casson nanofluid with Newtonian heating.

One of the greatest discoveries in material science history is carbon nanotubes (CNTs), which was discovered by a Japanese researcher in the beginning of the 1990s. Since the discovery, due to the unique electronic structural and mechanical characteristics, CNTs are found as valuable nanoparticles, especially in nanotechnology field. CNTs are great conductance which is highly sought in medical applications. They have been used as drug carriers and have benefited cancer therapy treatments [17]. The high thermal conductivity of CNTs has attracted significant attention from many researchers, including Xue [18], Khan et al. [19] and Saba et al. [20]. CNTs are hollow cylinders of carbon atoms in the forms of metals or semiconductors. CNTs are folded tubes of graphene sheet made up of hexagonal carbon rings, and their bundles are formed. CNTs are classified into two types with respectively differ in the graphene cylinder arrangement which are single-walled carbon nanotubes (SWCNTs) and multi-walled carbon nanotubes (MWCNTs). SWCNTs has one layer [21], while MWCNTs consist of more than one graphene cylinder layers [22]. Khalid et al. [23] studied the characteristics of flow and heat transfer for CNTs nanofluid affected by MHD and porosity effects. Acharya et al. [24] discussed a comparative study on the properties of MWCNTs and SWCNTs suspended in water with the imposition of magnetic field. The CNTs nanofluid flow induced by a moving plate was investigated by Anuar et al. [25] and a prominent effect on heat transfer and skin friction by SWCNTs was observed. Ebaid et al. [26] analyzed convective boundary layer for CNTs nanofluid under magnetic field

effect. The closed form solution was derived using Laplace transform method and the findings showed increasing magnetic strength and volume fraction of CNTs had deteriorated the rate of heat transport. Aman et al. [27] improved heat transfer for a Maxwell CNTs nanofluid moving over a vertical state plate with constant wall temperature. The investigation of velocity slip of carbon nanotubes flow with diffusion species was conducted by Hayat et al. [28]. Recently, the heat transmission analysis for water-based CNTs was discussed by Berrehal and Makinde [29], considering the flow over non-parallel plates and Ellahi et al. [30] considering flow past a truncated wavy cone.

Due to its broad range of uses such as car brake system, manufacturing of glass and plastic films, gas turbines, and medical equipment's, numerous researchers have effectively studied heat transfer and fluid flow in a rotation system [31]. The impact of MHD and porosity on rotating nanofluid flow with double diffusion by using regular nanoparticles was discussed by Krishna and Chamkha [32]. More features of heat transfer affected by porosity and magnetic field for a rotating fluid flow were referred in Das et al. [33] and Krishna et al. [34, 35]. Kumam et al. [36] implemented CNTs in analyzing the flow behavior for a rotating nanofluid. The nanofluid was considered as an electrical conducting fluid moving in a channel under heat source/sink and radiation effects. More study on the heat propagation for a convective flow of nanofluid in a rotating system affected by CNTs with several effects and different geometries were presented by Imtiaz et al. [37], Mosayebidorcheh and Hatami [38] and Acharya et al. [39]. Interestingly, several researchers had recently concentrated their study on the non-coaxial rotation flow. Mixer machines in food processing industry, cooling pad of electronic devices and rotating propellers for aircraft have become great application to exemplify the non-coaxial rotating phenomenon in various industries. Mohamad et al. [40] presented the mathematical expression for heat transfer in non-coaxial rotation of viscous fluid flow. As the extension of the previous study, the heat and mass transfer effects (double diffusion) were considered by Mohamad et al. [41] and followed by Mohamad et al. [42] investigating porosity effect in double diffusion flow of MHD fluid. Ersoy [43] imposed a disk with non-torsional oscillation to study the convective non-coaxial rotating flow for a Newtonian fluid. Mohamad et al. [44, 45] worked on similar study considering the second grade fluid and Rafiq et al. [46] concerning the Casson fluid model. The time dependent flow of an incompressible fluid with MHD, chemical reaction and radiation effects under non-coaxial rotation was investigated by Rana et al. [47]. Subjecting to the same type of rotation, Mohamad et al. [48] studied the porosity and MHD consequences in mixed convection flow influenced by an accelerated disk. The study was improved by Noranuar et al. [49] including the effects of double diffusive flow. According to the review of non-coaxial rotation, it is clear that most of the study are subjected to the ordinary fluid. However, the study of non-coaxial rotation for nanofluid by using regular nanoparticles had been performed by Das et al. [50] and Ashlin and Mahanthesh [51] but then the study reporting the implementation of CNTs in non-coaxial rotation flow remains limited.

Inspiring from the above literature, new study is essential to explore more findings on non-coaxial rotation of CNTs nanofluid. Therefore, the investigation of MHD non-coaxial rotating flow of CNTs nanofluid due to free convection in a porous medium become the primary focus of the current study. Water base fluid is chosen to suspend nanoparticle of SWCNTs and MWCNTs. The exact solutions for velocity and temperature distributions are attained by solving the problem analytically using the Laplace transform method. The results are illustrated in several graphs and tables for further analysis of various embedded parameters.

2. Problem formulation

The incompressible time-dependent carbon nanofluid instigated by non-coaxial rotation past a vertical disk with an impulsive motion is considered as illustrated in **Figure 1**, where x and z are the Cartesian coordinates with x-axis is chosen as the upward direction and z-axis is the normal of it. The semi-finite space $z > 0$ is occupied by nanofluid that composed by constant kinematic viscosity υ_{nf} of SWCNTs and MWCNTs suspended in water and acts as an electrically conducting fluid flowing through a porous medium. The disk is placed vertically along the x-axis with forward motion and a uniform transverse magnetic field of strength B_0 is applied orthogonal to it. The plane $x = 0$ is considered as rotation axes for both disk and fluid. Initially, at $t = 0$, the fluid and disk are retained at temperature T_∞ and rotate about z'-axis with the same angular velocity Ω. After time $t > 0$, the fluid remains rotating at z'-axis while the disk begins to move with velocity U_0 and rotates at z-axis. Both rotations have a uniform angular velocity Ω. The temperature of the disk raises to T_w and the distance between the two axes of rotation is equal to ℓ. With above assumptions, the usual Boussinesq approximation is applied, and the nanofluid model proposed by Tiwari and Das [52] is used to represent the problem in the governing equations, express as

$$\rho_{nf}\frac{\partial F}{\partial t} + \left(\rho_{nf}\Omega i + \sigma_{nf}B_0{}^2 + \frac{\mu_{nf}}{k_1}\right) = \mu_{nf}\frac{\partial^2 F}{\partial z^2} + (\rho\beta_T)_{nf}g_x(T - T_\infty)$$
$$+ \left(\rho_{nf}\Omega i + \sigma_{nf}B_0{}^2 + \frac{\mu_{nf}}{k_1}\right)\Omega\ell, \qquad (1)$$

$$\left(\rho C_p\right)_{nf}\frac{\partial T}{\partial t} = k_{nf}\frac{\partial^2 T}{\partial z^2}. \qquad (2)$$

The corresponding initial and boundary conditions are

$$F(z, 0) = \Omega\ell; \ T(z, 0) = T_\infty; z > 0,$$
$$F(0, t) = U_0; \ T(0, t) = T_w; t > 0, \qquad (3)$$
$$F(\infty, t) = \Omega\ell; \ T(\infty, t) = T_\infty; t > 0,$$

in which $F = f + ig$ is the complex velocity; f and g are (real) primary and (imaginary) secondary velocities respectively, T is the temperature of nanofluid and U_0 is the characteristic velocity. The following nanofluid constant for dynamic
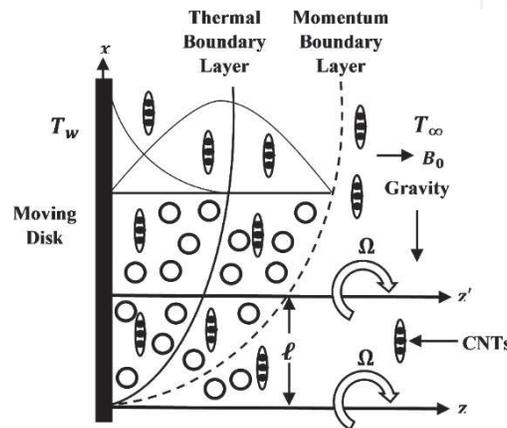

Figure 1.
Physical model of the problem.

viscosity μ_{nf}, density ρ_{nf}, heat capacitance $\left(\rho C_p\right)_{nf}$, electrical conductivity σ_{nf}, thermal expansion coefficient $(\beta_T)_{nf}$ and thermal conductivity k_{nf} can be used as

$$\mu_{nf} = \frac{\mu_f}{(1-\phi)^{2.5}}, \rho_{nf} = (1-\phi)\rho_f + \phi\rho_{CNTs},$$

$$\left(\rho C_P\right)_{nf} = (1-\phi)\left(\rho C_P\right)_f + \phi\left(\rho C_P\right)_{CNTs},$$

$$\frac{\sigma_{nf}}{\sigma_f} = 1 + \frac{3\left(\dfrac{\sigma_{CNTs}}{\sigma_f} - 1\right)\phi}{\left(\dfrac{\sigma_{CNTs}}{\sigma_f} + 2\right) - \phi\left(\dfrac{\sigma_{CNTs}}{\sigma_f} - 1\right)}, \tag{4}$$

$$(\beta_T)_{nf} = \frac{(1-\phi)(\rho\beta_T)_f + \phi(\rho\beta_T)_{CNTs}}{\rho_{nf}},$$

$$\frac{k_{nf}}{k_f} = \frac{1 - \phi + 2\phi\dfrac{k_{CNTs}}{k_{CNTs} - k_f}\ln\left(\dfrac{k_{CNTs} + k_f}{2k_f}\right)}{1 - \phi + 2\phi\dfrac{k_f}{k_{CNTs} - k_f}\ln\left(\dfrac{k_{CNTs} + k_f}{2k_f}\right)},$$

where the subscripts f is for fluid and *CNTs* is for carbon nanotubes. Meanwhile, ϕ is the solid volume fraction of nanofluid. The constants in Eq. (4) are used based on the thermophysical features in **Table 1**.

Introducing following dimensionless variables

$$F^* = \frac{F}{\Omega\ell} - 1, z^* = \sqrt{\frac{\Omega}{\upsilon}}z, t^* = \Omega t, T^* = \frac{T - T_\infty}{T_w - T_\infty}. \tag{5}$$

Using Eqs. (4) and (5), the governing equations in Eqs. (1)–(3) reduce to (excluding the * notation to simplify the equations)

$$\frac{\partial F}{\partial t} + d_1 F = \frac{1}{\phi_1}\frac{\partial^2 F}{\partial z^2} + \phi_3 GrT, \tag{6}$$

$$\frac{\partial T}{\partial t} = \frac{1}{a_1}\frac{\partial^2 T}{\partial z^2} \tag{7}$$

and the conditions take the form

$$F(z, 0) = 0, T(z, 0) = 0; z > 0,$$

$$F(0, t) = U - 1, T(0, t) = 1; t > 0, \tag{8}$$

$$F(\infty, t) = 0, T(\infty, t) = 0; t > 0,$$

Material	Properties				
	ρ (Kgm^{-3})	C_p $(JKg^{-1}K^{-1})$	k $(Wm^{-1}K^{-1})$	$\beta \times 10^{-5}$ (K^{-1})	σ (Sm^{-1})
Water	997.1	4179	0.613	21	0.05
SWCNTs	2600	425	6600	27	$10^6 - 10^7$
MWCNTs	1600	796	3000	44	1.9×10^{-4}

Table 1.
Thermophysical features of water, SWCNTs, and MWCNTs.

where

$$d_1 = \left(i + M^2 \phi_2 + \frac{1}{\phi_1 K} \right), a_1 = \frac{Pr \phi_4}{\lambda}, M = \frac{\sigma_f B_0{}^2}{\Omega \rho_f}, \frac{1}{K} = \frac{v_f}{k_1 \Omega},$$

$$\text{Pr} = \frac{v_f (\rho C_p)_f}{k_f}, Gr = \frac{g_x \beta_{Tf} (T_w - T_\infty)}{\Omega^2 \ell}, U = \frac{U_0}{\Omega \ell}. \tag{9}$$

At this point, d_1 and a_1 are constant parameters, M is the magnetic parameter (magnetic field), K is the porosity parameter, Pr is Prandtl number, Gr is Grashof number and U is the amplitude of disk. Besides that, the other constant parameters are

$$\lambda = \frac{k_{nf}}{k_f}, \phi_1 = (1 - \phi)^{2.5} \left((1 - \phi) + \frac{\phi \rho_{CNTs}}{\rho_f} \right),$$

$$\phi_2 = \left(1 + \frac{3 \left(\frac{\sigma_{CNTs}}{\sigma_f} - 1 \right) \phi}{\left(\frac{\sigma_{CNTs}}{\sigma_f} + 2 \right) - \phi \left(\frac{\sigma_{CNTs}}{\sigma_f} - 1 \right)} \right) \frac{1}{\left((1 - \phi) + \frac{\phi \rho_{CNTs}}{\rho_f} \right)}, \tag{10}$$

$$\phi_3 = \frac{(1 - \phi) + \frac{\phi (\rho \beta)_{CNTs}}{(\rho \beta)_f}}{(1 - \phi) + \frac{\phi \rho_{CNTs}}{\rho_f}}, \phi_4 = (1 - \phi) + \frac{\phi (\rho C_p)_{CNTs}}{(\rho C_p)_f}.$$

3. Exact solution

Next, the system of equations in Eqs. (6)–(8) after applying Laplace transform yield to the following form

$$\frac{d^2}{dz^2} \overline{F}(z, q) - (\phi_1 q + d_2) \overline{F}(z, q) = -d_3 Gr \overline{T}(z, q), \tag{11}$$

$$\overline{F}(0, q) = (U - 1) \frac{1}{q}, \overline{F}(\infty, q) = 0, \tag{12}$$

$$\frac{d^2}{dz^2} \overline{T}(z, q) - (a_1 q) \overline{T}(z, q) = 0, \tag{13}$$

$$\overline{T}(0, q) = \frac{1}{q}, \overline{T}(\infty, q) = 0. \tag{14}$$

Then, Eqs. (11) and (13) are solved by using the boundary conditions, Eqs. (12) and (14). After taking some manipulations on the resultant solutions, the following Laplace solutions form

$$\overline{F}(z, q) = \overline{F}_1(z, q) - \overline{F}_2(z, q) - \overline{F}_3(z, q) + \overline{F}_4(z, q) + \overline{F}_5(z, q) - \overline{F}_6(z, q), \tag{15}$$

$$\overline{T}(z, q) = \frac{1}{q} exp \left(-z \sqrt{a_1 q} \right), \tag{16}$$

where

$$\overline{F}_1(z,q) = \frac{U}{q} \exp\left(-z\sqrt{\phi_1 q + d_2}\right), \overline{F}_2(z,q) = \frac{1}{q} \exp\left(-z\sqrt{\phi_1 q + d_2}\right),$$

$$\overline{F}_3(z,q) = \frac{a_4}{q} \exp\left(-z\sqrt{\phi_1 q + d_2}\right), \overline{F}_4(z,q) = \frac{a_4}{q - a_3} \exp\left(-z\sqrt{\phi_1 q + d_2}\right),$$

$$\overline{F}_5(z,q) = \frac{a_4}{q} \exp\left(-z\sqrt{a_1 q}\right), \overline{F}_6(z,q) = \frac{a_4}{q - a_3} \exp\left(-z\sqrt{a_1 q}\right)$$

$$(17)$$

are defined, respectively. The exact solutions for the temperature and velocity are finally generated by utilizing the inverse Laplace transform on Eqs. (15) and (16). Hence, it results

$$F(z,t) = F_1(z,t) - F_2(z,t) - F_3(z,t) + F_4(z,t) + F_5(z,t) - F_6(z,t) \qquad (18)$$

$$T(z,t) = erfc\left(\frac{z}{2}\sqrt{\frac{a_1}{t}}\right) \qquad (19)$$

with

$$F_1(z,t) = \frac{U}{2} \exp\left(z\sqrt{\phi_1 d_4}\right) erfc\left(\frac{z}{2}\sqrt{\frac{\phi_1}{t}} + \sqrt{d_4 t}\right)$$
$$+ \frac{U}{2} \exp\left(-z\sqrt{\phi_1 d_4}\right) erfc\left(\frac{z}{2}\sqrt{\frac{\phi_1}{t}} - \sqrt{d_4 t}\right),$$

$$F_2(z,t) = \frac{1}{2} \exp\left(z\sqrt{\phi_1 d_4}\right) erfc\left(\frac{z}{2}\sqrt{\frac{\phi_1}{t}} + \sqrt{d_4 t}\right)$$
$$+ \frac{1}{2} \exp\left(-z\sqrt{\phi_1 d_4}\right) erfc\left(\frac{z}{2}\sqrt{\frac{\phi_1}{t}} - \sqrt{d_4 t}\right),$$

$$F_3(z,t) = \frac{a_4}{2} \exp\left(z\sqrt{\phi_1 d_4}\right) erfc\left(\frac{z}{2}\sqrt{\frac{\phi_1}{t}} + \sqrt{d_4 t}\right)$$
$$+ \frac{a_4}{2} \exp\left(-z\sqrt{\phi_1 d_4}\right) erfc\left(\frac{z}{2}\sqrt{\frac{\phi_1}{t}} - \sqrt{d_4 t}\right), \qquad (20)$$

$$F_4(z,t) = \frac{a_4}{2} \exp\left(a_3 t + z\sqrt{\phi_1(a_3 + d_4)}\right) erfc\left(\frac{z}{2}\sqrt{\frac{\phi_1}{t}} + \sqrt{(a_3 + d_4)t}\right)$$
$$+ \frac{a_4}{2} \exp\left(a_3 t - z\sqrt{\phi_1(a_3 + d_4)}\right) erfc\left(\frac{z}{2}\sqrt{\frac{\phi_1}{t}} - \sqrt{(a_3 + d_4)t}\right),$$

$$F_5(z,t) = a_4 erfc\left(\frac{z}{2}\sqrt{\frac{a_1}{t}}\right),$$

$$F_6(z,t) = \frac{a_4}{2} \exp\left(a_3 t + z\sqrt{a_1 a_3}\right) erfc\left(\frac{z}{2}\sqrt{\frac{a_1}{t}} + \sqrt{a_3 t}\right)$$
$$+ \frac{a_4}{2} \exp\left(a_3 t - z\sqrt{a_1 a_3}\right) erfc\left(\frac{z}{2}\sqrt{\frac{a_1}{t}} - \sqrt{a_3 t}\right),$$

where

$$d_2 = \phi_1 d_1, d_3 = \phi_1 \phi_3, d_4 = \frac{d_2}{\phi_1}, a_2 = a_1 - \phi_1, a_3 = \frac{d_2}{a_2}, a_4 = \frac{d_3 Gr}{a_2 a_3}. \qquad (21)$$

4. Physical quantities

In this study, the skin friction $\tau(t)$ and Nusselt number Nu for the flow of Newtonian nanofluid in non-coaxial rotation are also analyzed. Their dimensional form is expressed as

$$\tau(t) = -\mu_{nf} \left. \frac{\partial F}{\partial z} \right|_{z=0} \qquad (22)$$

$$Nu = -k_{nf} \left. \frac{\partial T}{\partial z} \right|_{z=0} \qquad (23)$$

Incorporating Eqs. (22) and (23) with the nanofluid model Eq. (4), dimensionless variables Eq. (5) and solutions Eqs. (18) and (19), the following dimensionless skin friction and Nusselt number form as

$$
\begin{aligned}
\tau(t) &= -\frac{1}{(1-\phi)^{2.5}} \left. \frac{\partial F}{\partial z} \right|_{z=0}, \\
&= -\frac{1}{(1-\phi)^{2.5}} (\tau_1(t) - \tau_2(t) - \tau_3(t) + \tau_4(t) - \tau_5(t) + \tau_6(t)),
\end{aligned} \qquad (24)
$$

$$Nu = -\frac{k_{nf}}{k_f} \left. \frac{\partial T}{\partial z} \right|_{z=0} = \lambda \sqrt{\frac{a_1}{\pi t}}, \qquad (25)$$

where

$$\tau_1(t) = U\sqrt{\phi_1 d_4}\,\text{erfc}\left(\sqrt{d_4 t}\right) - U\sqrt{\phi_1 d_4} - \frac{U}{2}\sqrt{\frac{\phi_1}{\pi t}}\exp\left(-d_4 t\right),$$

$$\tau_2(t) = \sqrt{\phi_1 d_4}\,\text{erfc}\left(\sqrt{d_4 t}\right) - \sqrt{\phi_1 d_4} - \sqrt{\frac{\phi_1}{\pi t}}\exp\left(-d_4 t\right),$$

$$\tau_3(t) = a_4\sqrt{\phi_1 d_4}\,\text{erfc}\left(\sqrt{d_4 t}\right) - a_4\sqrt{\phi_1 d_4} - a_4\sqrt{\frac{\phi_1}{\pi t}}\exp\left(-d_4 t\right),$$

$$
\begin{aligned}
\tau_4(t) &= a_4\sqrt{\phi_1(a_3 + d_4)}\exp\left(a_3 t\right)\text{erfc}\left(\sqrt{(a_3 + d_4)t}\right) - a_4\sqrt{\frac{\phi_1}{\pi t}}\exp\left(-d_4 t\right) \\
&\quad - a_4\sqrt{\phi_1(a_3 + d_4)}\exp\left(a_3 t\right),
\end{aligned} \qquad (26)
$$

$$\tau_5(t) = -a_4\sqrt{\frac{a_1}{\pi t}},$$

$$\tau_6(t) = a_4\sqrt{a_1 a_3}\exp\left(a_3 t\right)\text{erfc}\left(\sqrt{a_3 t}\right) - a_4\sqrt{a_1 a_3}\exp\left(a_3 t\right) - a_4\sqrt{\frac{a_1}{\pi t}},$$

with $\tau^* = \tau\sqrt{\nu_f}/_{\mu_f \Omega^{\frac{3}{2}}\ell}$.

5. Analysis of results

The dimensionless differential equations of non-coaxial rotating nanofluid flow with associated boundary and initial conditions are analytically solved using the method of Laplace transform to obtain the closed form solutions of heat transfer. Further analysis for the role of dimensionless time t, Grashof number Gr, volume fraction of nanoparticles ϕ, porosity parameter K, magnetic field parameter M and amplitude of disk U on velocity and temperature distributions as well as Nusselt number and skin friction are presented in figures and tables. The profiles are plotted with the physical value of parameters as $\Pr = 6.2, Gr = 0.5, M = 0.2, K = 2.0, \phi = 0.02, U = 2.0$ and $t = 0.2$. The values are same unless for the investigated parameter of the profile. Since the rotating nanofluid is part of the problem, the results are discussed by presenting the graph of velocity profile in real and imaginary parts, specifically describes the primary f and secondary g velocities. The velocity profiles are demonstrated in **Figures 2**–**7** and the temperature profiles are illustrated in **Figures 8** and **9**. From these profiles, it is found that all the obtained results satisfy both boundary and initial conditions. SWCNTs and MWCNTs have an identical nature of fluid flow and heat transfer.

Figure 2 depicts the plotting of f and g profiles with varying t values. Overall, the velocity of both SWCNTs and MWCNTs rises over time. As t increases, the buoyancy force becomes more effective and functions as an external source of energy to the flow, causing the velocity of fluid to increase. **Figure 3** illustrates the variation of f and g profiles for SWCNTs and MWCNTs cases under the effect of Gr. It is essential to note that Gr is an approximation of the buoyancy force to the viscous force exerting on the flow. Hence, an increase of Gr suggests to the domination of
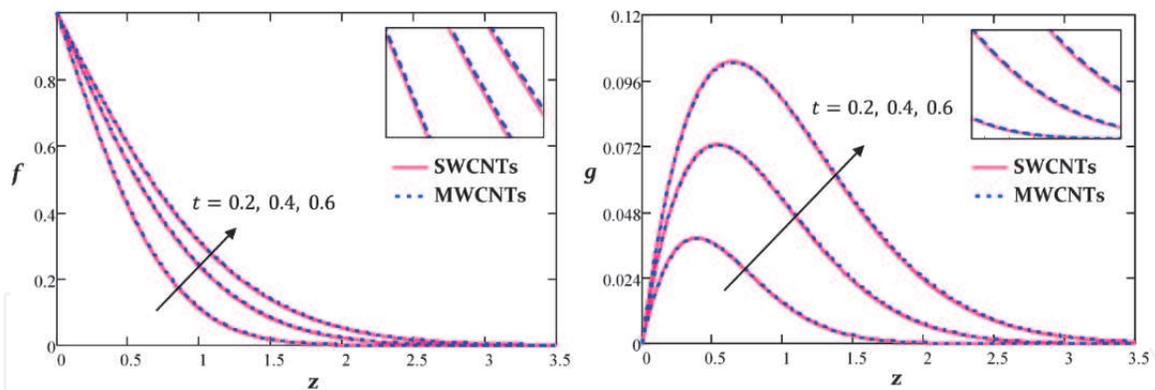

Figure 2.
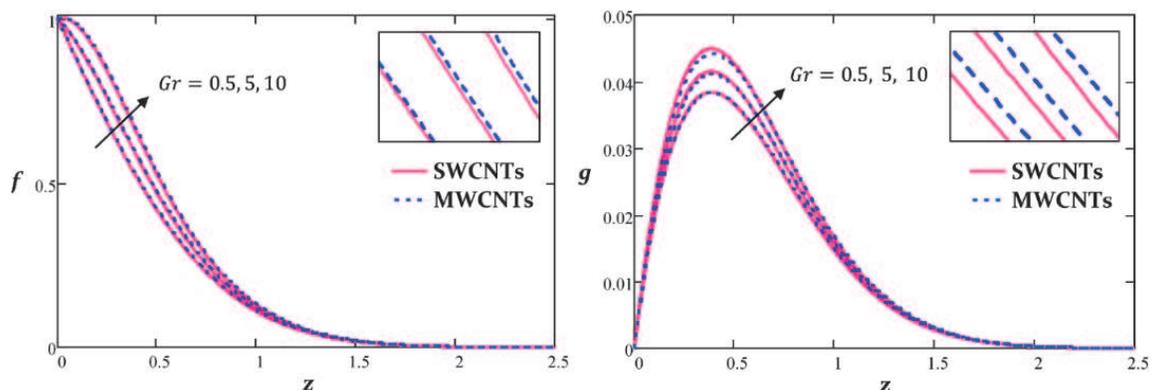*Profile of f and g for varied values of t.*

Figure 3.
Profile of f and g for varied values of Gr.
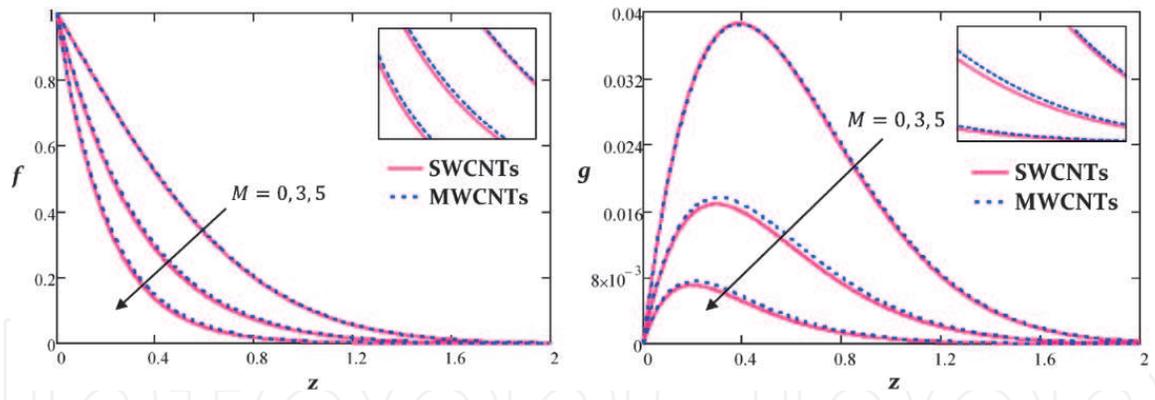
Figure 4.
Profile of f and g for varied values of M.
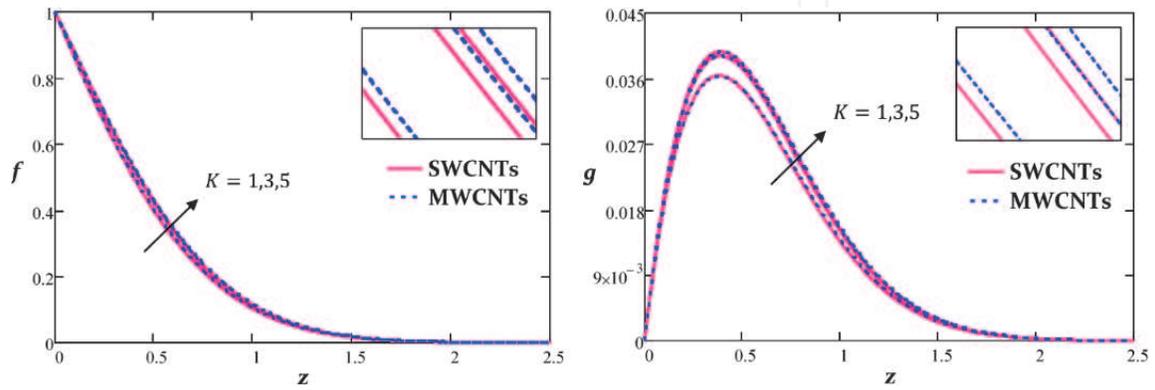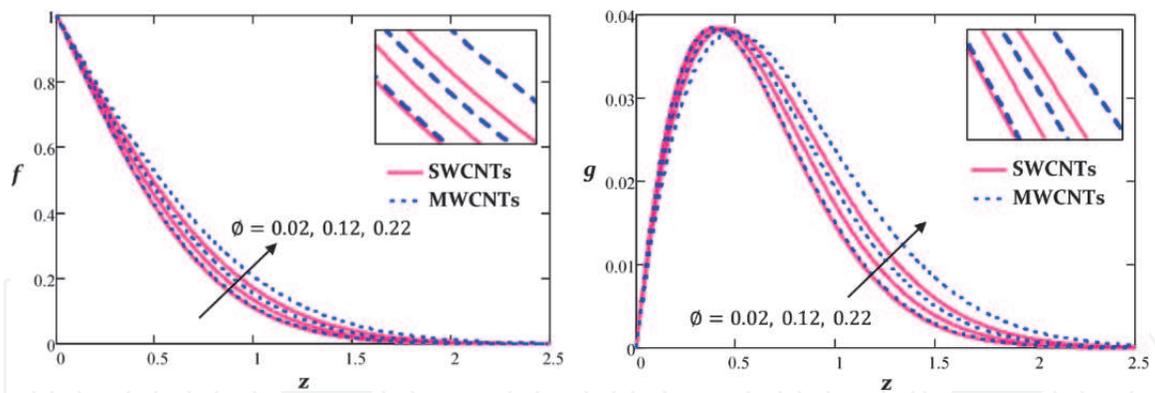

Figure 5.
Profile of f and g for varied values of K.
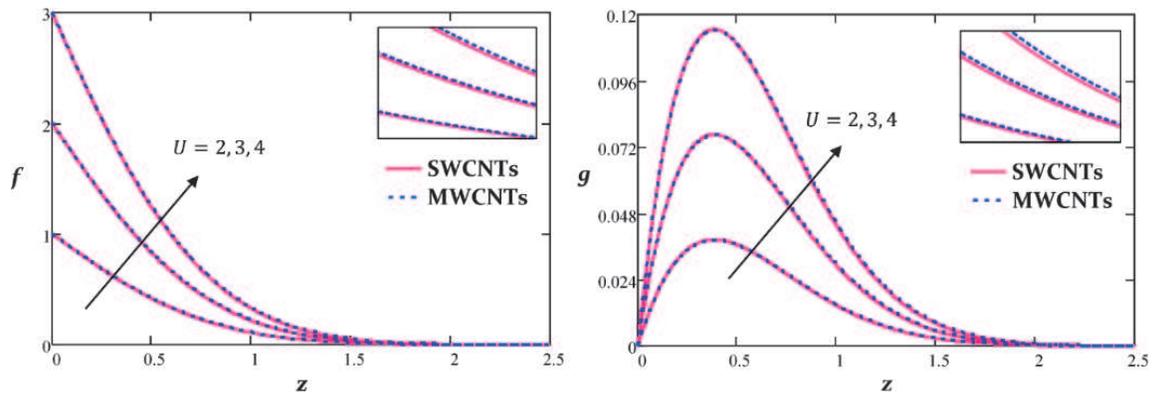

Figure 6.
Profile of f and g for varied values of φ.

Figure 7.
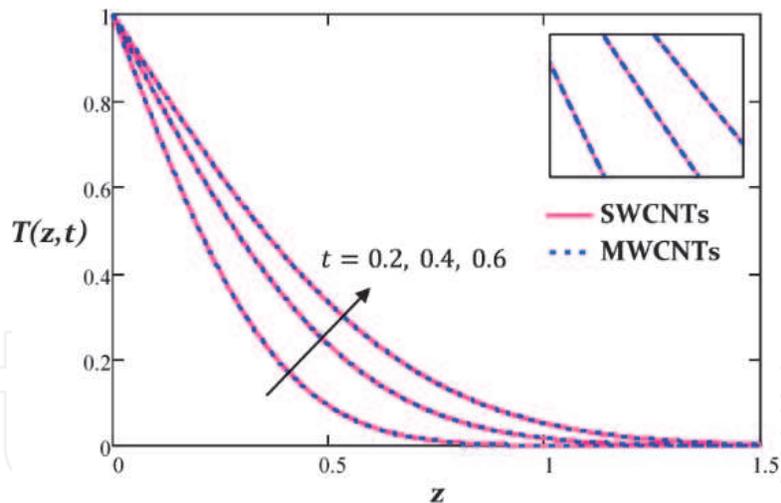*Profile of f and g for varied values of U.*

Figure 8.
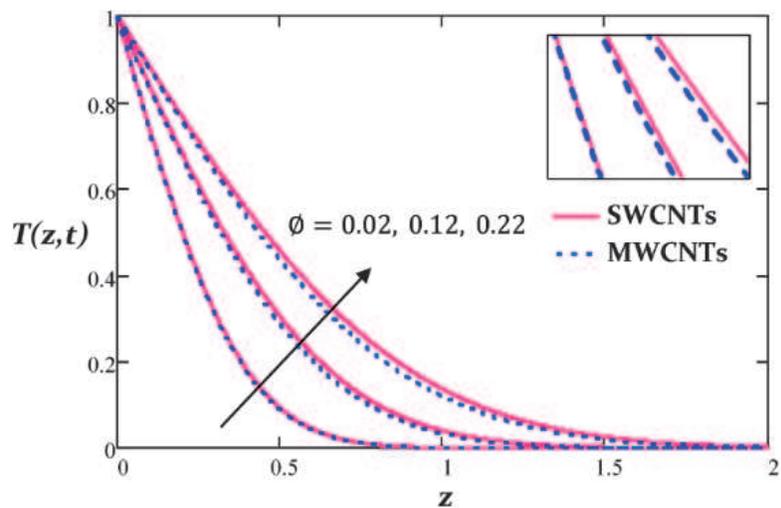*Profile of $T(z,t)$ for varied values of t.*

Figure 9.
Profile of $T(z,t)$ for varied values of ϕ.

buoyancy force and reduces the viscosity of fluid. Thus, growing *Gr* leads to an augment of fluid velocity.

On the other hand, **Figure 4** discloses the nature of fluid flow in response to *M*. For both SWCNTs and MWCNTs cases, the figure suggests that amplifying *M* decreases *f* and *g* profiles. This impact is owing to the fact that a greater *M* value increases the frictional forces acting on the fluid, commonly known as the Lorentz force. Consequently, the fluid encounters substantial resistance along the flow and its velocity decreases. Next, the contribution of *K* in SWCNTs and MWCNTs nanofluids for both *f* and *g* profiles are displayed in **Figure 5**. It suggests that *K* value increases linearly with the velocities for both SWCNTs and MWCNTs. Noting that porosity is also greatly affected by the permeability of a medium, where it determines the ability of a medium to enable the fluid to flow through it. Then, the increasing values of *K* cause the medium to be more permeable and the fluid can easily pass through the medium. Therefore, it increases both *f* and *g* profiles.

Figure 6 reveals the consequences of *φ* on *f* and *g* profiles in the cases of SWCNTs and MWCNTs. It shows that increasing *φ* values result in the increment of *f* profiles and fluctuating trend of *g* profiles. This suggests significant advantages of non-coaxial rotation in CNTs, especially in industrial and medical applications. In line with a general finding, an analysis proceeding in cancer treatment has reported

that the CNTs with higher velocity have been used to reach the tumor's site. Besides, referring to **Figure 7**, it is noticed that ascending U also has a positive impact on velocity profiles for both CNTs suspensions, where the velocity ascends linearly with the values of U. As U increases, this proposes to the creation of external sources, which are used to enhance the thrust force acting in the fluid flow. Thus, the velocity fluid elevates with increasing U.

Furthermore, the temperature profiles $T(z,t)$ under the impacts of t and ϕ are displayed graphically in **Figures 8** and **9**. It reveals that increment of t and ϕ contributes to a rise in nanofluid temperature for both types of CNTs case and followed by the magnification of thermal boundary layer. Physically, the addition of sufficient ϕ of CNTs can improve nanofluid's thermal conductivity. The more CNTs being inserted, the higher the thermal conductivity, which unsurprisingly improves the ability of fluid to conduct heat. Therefore, a growth of temperature profile is exhibited for increasing ϕ. The comparison of physical behavior for SWCNTs and MWCNTs are clearer when referring to the zooming box of each graph. Overall, **Figures 2**–**7** reveal that the velocity profile of MWCNTs case is more significant compared to the velocity of SWCNTs. This behavior is agreed to the thermophysical features in **Table 1**, where MWCNTs have low density, which also being a key factor for the increase of velocity profiles. Meanwhile, from **Figures 8** and **9**, SWCNTs have provided a prominent effect on temperature profiles as it is affected by a high thermal conductivity property.

t	Gr	M	K	ϕ	U	SWCNTs		MWCNTs	
						τ_p	τ_s	τ_p	τ_s
0.2	**0.5**	**0.2**	**2**	**0.02**	**2**	1.3811	-0.2550	1.3691	-0.2523
0.4	0.5	0.2	2	0.02	2	1.0318	-0.3492	1.0236	-0.3455
0.2	**5**	0.2	2	0.02	2	0.6276	-0.2705	0.6195	-0.2676
0.2	0.5	**3**	2	0.02	2	3.2171	-0.1596	3.0871	-0.1620
0.2	0.5	0.2	**3**	0.02	2	1.3377	-0.2578	1.3252	-0.2552
0.2	0.5	0.2	2	**0.12**	2	1.6820	-0.3138	1.6016	-0.2966
0.2	0.5	0.2	2	0.02	**3**	2.8459	-0.5082	2.8214	-0.5030

*The significance of bold emphasis used in **Table 2** is for the comparison of the effects for varied values of the particular parameters. For each parameter, the changes of skin friction values are compared among the bold values of parameters.*

Table 2.
Values of primary τ_p and secondary τ_s skin friction for SWCNTs and MWCNTs.

t	ϕ	Nu	
		SWCNTs	MWCNTs
0.2	**0.02**	3.6238	3.5818
0.4	0.02	2.5624	2.5327
0.2	**0.12**	5.4840	5.3185

*The significance of bold emphasis used in **Table 3** is for the comparison of the effects for varied values of the particular parameters. For each parameter, the changes of Nusselt number values are compared among the bold values of parameters.*

Table 3.
Values of Nusselt number Nu for SWCNTs and MWCNTs.

Tables 2 and **3** show the results of skin friction (τ_p and τ_s) and Nusselt number Nu for various parameters on both cases SWCNTs and MWCNTs. According to **Table 2**, it shows that both τ_p and τ_s of SWCNTs and MWCNTs rise when the strength of M higher. These effects cause the surface to produce high friction drag due to the maximization of wall shear stress. On the contrary, as Gr, K and t increase, both suspension of SWCNTs and MWCNTs report a diminution in τ_p and τ_s. This shows that augmentation of Gr, K and t have reduced the friction between fluid and surfaces which lead the velocity to increase. Meanwhile, as ϕ and U increase, both suspension of SWCNTs and MWCNTs report a growth of τ_p and a diminution in τ_s. From **Table 3**, it shows that Nu for both CNTs cases decrease as the values of t increase. However, when involving high ϕ, both SWCNTs and MWCNTs have large Nu which also implies to have a great of heat transfer rate. This effect is also directly affected by the reduction of nanofluid heat capacitance as ϕ increases. Overall, for **Table 3**, it is found that SWCNTs case have high value of Nu compared to MWCNTs, due to its reduction of heat capacitance. This effect also signifies for a better heat transfer process that can be used in several engineering and industrial system.
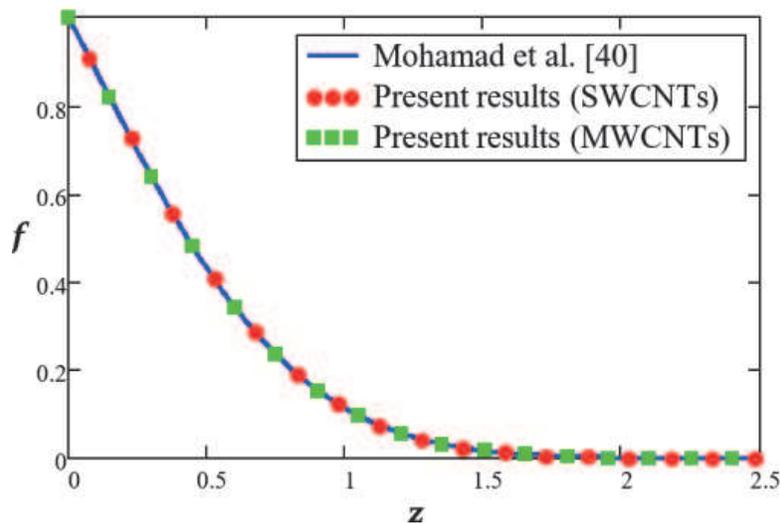

Figure 10.
Comparison of f profiles from present results in Eq. (18) with the published work by Mohamad et al. [40] in Eq. (53).
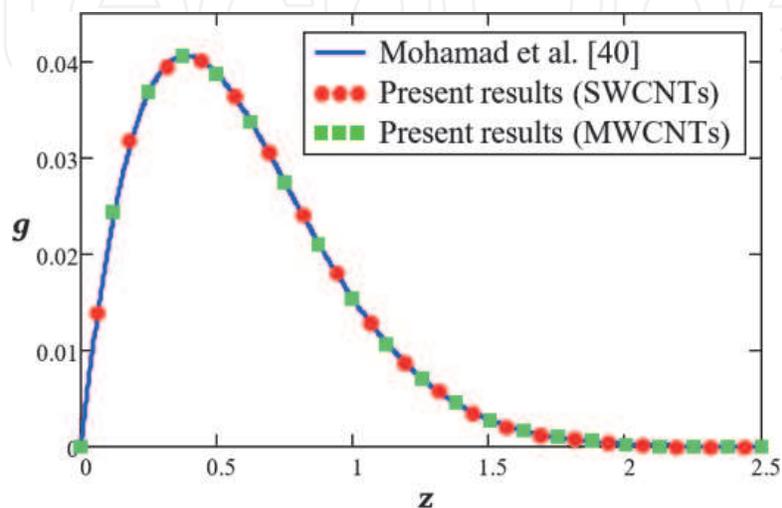

Figure 11.
Comparison of g profiles from present results in Eq. (18) with the published work by Mohamad et al. [40] in Eq. (53).

z	Exact Eq. (18)		Numerical Laplace Eq. (15)	
	SWCNTs	MWCNTs	SWCNTs	MWCNTs
0	1.0000	1.0000	1.0000	1.0000
0.5	0.4165	0.4206	0.4165	0.4206
1.0	0.1089	0.1122	0.1089	0.1121
1.5	0.0171	0.0182	0.0172	0.0182
2.0	0.0016	0.0017	0.0015	0.0017

Table 4.
*Comparison of exact and numerical solution of f profiles for SWCNTs and MWCNTs with
$t = 0.2, Gr = 0.5, M = 0.2, K = 2, \phi = 0.02, U = 2, Pr = 6.2$.*

z	Exact Eq. (18)		Numerical Laplace Eq. (15)	
	SWCNTs	MWCNTs	SWCNTs	SWCNTs
0	0.0000	0.0000	0.0000	0.0000
0.5	0.0366	0.0367	0.0366	0.0367
1.0	0.0146	0.0149	0.0146	0.0150
1.5	0.0027	0.0029	0.0027	0.0029
2.0	0.0003	0.0003	0.0003	0.0003

Table 5.
*Comparison of exact and numerical solution of g profiles for SWCNTs and MWCNTs with
$t = 0.2, Gr = 0.5, M = 0.2, K = 2, \phi = 0.02, U = 2, Pr = 6.2$.*

The accuracy of the obtained solution is verified by comparing solution in Eq. (18) with the solution obtained by Mohamad et al. [40] in Eq. (53). The comparison is conducted by letting magnetic parameter and nanoparticle volume fraction $M = \phi = 0$, and porosity parameter $K \rightarrow \infty$ in the present solution for both types of CNTs and letting phase angle $\omega = 0$ and amplitude of disk oscillation $U = 2$ in the published work. This comparison shows that f and g profiles for both present and previous works are identical to each other as clearly presented in **Figures 10** and **11**, which thus proves that the accuracy of obtained solution is verified. Meanwhile, another verification is also carried out to verify the validity of present solution by comparing the values of velocity profiles from the present work with the numerical values solved by numerical Gaver-Stehfest algorithm [53, 54]. **Tables 4** and **5** observe that the results of f and g profiles from the exact solution in Eq. (18) and the results from numerical solution are in excellent agreement.

6. Summary with conclusion

The unsteady non-coaxial rotation of water-CNTs nanofluid flow in a porous medium with MHD effect is analytically solved for the exact solutions by applying the Laplace transform method. The temperature and velocity profiles with various values of parameter for the immersion of SWCNTs and MWCNTs are plotted graphically and analyzed for their effects. From the discussion, significant findings emerge:

1. Both primary and secondary velocities for SWCNTs and MWCNTs suspension increase as the values of $t, Gr, K,$ and U increase while decrease as the values of M increase.

2. The insertion of higher ϕ of SWCNTs and MWCNTs increases the primary velocity profiles while for secondary velocity profiles, fluctuating trend is reported for both cases.

3. The temperature of nanofluid increases when ϕ and t increase for both SWCNTs and MWCNTs cases.

4. MWCNTs have higher primary and secondary velocity profiles compared to SWCNTs because of their low-density property

5. SWCNTs have higher temperature profile than MWCNTs owing to their high thermal conductivity property.

6. The increasing values of t, Gr and K decrease both primary and secondary skin friction for both types of CNTs while the increase of M gives opposite effect on both skin friction.

7. Nusselt number for both CNTs cases reduce as t increases and amplify as ϕ increases.

8. The findings in present work are in accordance to findings in Mohamad et al. [40] and numerical values obtained by numerical Gaver-Stehfest algorithm.

Acknowledgements

Conflict of interest

The authors declare that they have no conflicts of interest to report regarding the present study.

Nomenclature

β_T	Thermal expansion coefficient
C_p	Specific heat
ρ	Density
σ	Electrical conductivity
μ	Dynamic viscosity
g_x	Acceleration due to gravity
k	Thermal conductivity
T	Temperature of nanofluid

T_∞	Free stream temperature
T_w	Wall temperature
B_0	Magnetic field
k_1	Permeability
U_0	Characteristic of velocity
Nu	Nusselt number
τ	Skin friction
τ_p	Primary skin friction
τ_s	Secondary skin friction
F	Complex velocity
f	Primary velocity
g	Secondary velocity
ϕ	Volume fraction nanoparticles
Ω	Angular velocity
t	Time
i	Imaginary unit
Pr	Prandtl number
Gr	Grashof number
K	Porosity

Subscripts

CNTs	Carbon nanotubes
nf	Nanofluid
f	Fluid

Author details

Wan Nura'in Nabilah Noranuar[1], Ahmad Qushairi Mohamad[1*], Sharidan Shafie[1], Ilyas Khan[2], Mohd Rijal Ilias[3] and Lim Yeou Jiann[1]

1 Faculty of Science, Department of Mathematical Sciences, Universiti Teknologi Malaysia, Johor Bahru, Malaysia

2 Faculty of Mathematics and Statistics, Ton Duc Thang University, Ho Chi Minh City, Vietnam

3 Faculty of Computer and Mathematical Sciences, Centre of Mathematics Studies, Universiti Teknologi MARA (UiTM), Shah Alam, Selangor, Malaysia

*Address all correspondence to: ahmadqushairi@utm.my

IntechOpen

References

[1] Sivashanmugam P. Application of nanofluids in heat transfer, In: S. N. Kazi (Ed.), An Overview of Heat Transfer, INTECH Publications, Croatia, 2012, 411-440.

[2] Choi SUS, Eastman JA. Enhancing thermal conductivity of fluids with nanoparticles, United States, 1995.

[3] Azhar WA, Vieru D, Fetecau C. Free convection flow of some fractional nanofluids over a moving vertical plate with uniform heat flux and heat source. Physics of Fluids. 2017:29(9):1-13. DOI: http://dx.doi.org/10.1063/1.4996034

[4] Gbadeyan JA, Titiloye EO, Adeosun AT. Effect of variable thermal conductivity and viscosity on Casson nanofluid flow with convective heating and velocity slip. Heliyon. 2020:6: e03076. DOI: https://doi.org/10.1016/j.heliyon.2019.e03076

[5] Rehman F, Khan MI, Sadiq M, Malook A. MHD flow of carbon in micropolar nanofluid with convective heat transfer in the rotating frame. Journal of Molecular Liquids. 2017:231:353-263. DOI: 10.1016/j.molliq.2017.02.022

[6] Sulochana C, Ashwinkumar GP, Sandeep N. Effect of frictional heating on mixed convection flow of chemically reacting radiative Casson nanofluid over an inclined porous plate. Alexandria Engineering Journal. 2018:57(4): 2573-2584. DOI: http://dx.doi.org/10.1016/j.aej.2017.08.006

[7] Sandeep N, Reddy MG. Heat transfer of nonlinear radiative magnetohydrodynamic Cu-water nanofluid flow over two different geometries. Journal of Molecular Liquids. 2017:225:87-94. DOI: http://dx.doi.org/10.1016/j.molliq.2016.11.026

[8] Abbas W, Magdy MM. Heat and mass transfer analysis of nanofluid flow based on Cu, Al2O3, and TiO2 over a moving rotating plate and impact of various nanoparticle shapes. Mathematical Problems in Engineering. 2020:2020:1-12. DOI: https://doi.org/10.1155/2020/9606382

[9] Anwar T, Kumam P, Watthayu W. An exact analysis of unsteady MHD free convection flow of some nanofluids with ramped wall velocity and ramped wall temperature accounting heat radiation and injection/consumption. Scientific Reports. 2020:10(1):1-19. DOI: https://doi.org/10.1038/s41598-020-74739-w

[10] Benos L, Sarris IE. Analytical study of the magnetohydrodynamic natural convection of a nanofluid filled horizontal shallow cavity with internal heat generation. International Journal of Heat and Mass Transfer. 2019:130: 862-873. DOI: https://doi.org/10.1016/j.ijheatmasstransfer.2018.11.004

[11] Hussanan A, Salleh MZ, Khan I, Chen ZM. Unsteady water functionalized oxide and non-oxide nanofluids flow over an infinite accelerated plate. Chinese Journal of Physics. 2019:62:115-131. DOI: https://doi.org/10.1016/j.cjph.2019.09.020

[12] Prasad PD, Kumar RVMSSK, Varma SVK. Heat and mass transfer analysis for the MHD flow of nanofluid with radiation absorption. Ain Shams Engineering Journal. 2018:9(4):801-813. DOI: http://dx.doi.org/10.1016/j.asej.2016.04.016

[13] Anwar T, Kumam P, Shah Z, Watthayu W, Thounthong P. Unsteady radiative natural convective MHD nanofluid flow past a porous moving vertical plate with heat source/sink. Molecules. 2020:25(4):1-21. DOI: 10.3390/molecules25040854

[14] Coa Z, Zhoa J, Wang Z, Liu F, Zheng L. MHD flow and heat transfer of

fractional Maxwell viscoelastic nanofluid over a moving plate. Journal of Molecular Liquids. 2016:222: 1121-1127. DOI: 10.1016/j. molliq.2016.08.012

[15] Ramzan M, Bilal M, Chung JD, Mann AB. On MHD radiative Jeffery nanofluid flow with convective heat and mass boundary conditions. Neural Computing and Applications. 2017:30 (9):2739-2748. DOI: https://doi.org/ 10.1007/s00521-017-2852-8

[16] Khan A, Khan D, Khan I, Ali F, Karim FU, Imran M. MHD flow of sodium alginate-based Casson type nanofluid passing through a porous medium with Newtonian heating, Scientific Reports. 2018:8(1):1-18. DOI: 10.1038/s41598-018-26994-1

[17] Saleh H, Alali E, Ebaid A. Medical applications for the flow of carbon-nanotubes suspended nanofluids in the presence of convective condition using Laplace transform. Journal of the Association of Arab Universities for Basic and Applied Sciences. 2017:24: 206-212. DOI: http://dx.doi.org/ 10.1016/j.jaubas.2016.12.001

[18] Xue QZ. Model for thermal conductivity of carbon nanotubes-based composites. Physica B: Condensed Matter. 2005:368(1–4):302-307. DOI: 10.1016/j.physb.2005.07.024

[19] Khan ZH, Khan WA, Haq RU, Usman M, Hamid M. Effects of volume fraction on water-based carbon nanotubes flow in a right-angle trapezoidal cavity: FEM based analysis. International Communications in Heat and Mass Transfer. 2020:116:1-10. DOI: https://doi.org/10.1016/j.icheatmasstransfer.2020.104640

[20] Saba F, Ahmed N, Hussain S, Khan U, Mohyud-Din ST, Darus M. Thermal analysis of nanofluid flow over a curved stretching surface suspended by carbon nanotubes with internal heat

generation. Applied Sciences. 2018:8(3): 395. DOI: https://doi.org/10.3390/app8030395

[21] Pham VP, Jo YW, Oh JS, Kim SM, Park JW, Kim SH, Jhon MS, Yeom GY. Effect of plasma-nitric acid treatment on the electrical conductivity of flexible transparent conductive films. Japanese Journal of Applied Physics. 2013:52(7R): 075102. DOI: http://dx.doi.org/10.7567/JJAP.52.075102

[22] Ellahi R, Hassan M, Zeeshan A. Study of natural convection MHD nanofluid by means of single and multi-walled carbon nanotubes suspended in a salt water solution. IEEE Transactions on Nanotechnology. 2015:14(4):726-734. DOI: 10.1109/TNANO.2015.2435899

[23] Khalid A, Khan I, Khan A, Shafie S, Tlili I. Case study of MHD blood flow in a porous medium with CNTS and thermal analysis. Case Studies in Thermal Engineering. 2018:12:374-380. DOI: https://doi.org/10.1016/j.csite.2018.04.004

[24] Acharya N, Bag R, Kundu PK. On the mixed convective carbon nanotube flow over a convectively heated curved surface Heat Transfer. 2020:49(4): 1713-1735. DOI: 10.1002/htj.21687

[25] Anuar N, Bachok N, Pop I. A stability analysis of solutions in boundary layer flow and heat transfer of carbon nanotubes over a moving plate with slip effect. Energies. 2018:11(12): 1-20. DOI: 10.3390/en11123243

[26] Ebaid A, Al Sharif MA. Application of Laplace transform for the exact effect of a magnetic field on heat transfer of carbon nanotubes-suspended nanofluids. Zeitschrift für Naturforschung A. 2015:70(6):471-475. DOI: 10.1515/zna-2015-0125

[27] Aman S, Khan I, Ismail Z, Salleh MZ, Al-Mdallal QM. Heat transfer enhancement in free

convection flow of CNTS Maxwell nanofluids with four different types of molecular liquids. Scientific Reports. 2017:7(1):2445. DOI: 10.1038/s41598-017-01358-3

[28] Hayat T, Hussain Z, Alsaedi A, Hobiny A. Computational analysis for velocity slip and diffusion species with carbon nanotubes. Results in Physics. 2017:7(1):3049-3058. DOI: http://dx.doi.org/10.1016/j.rinp.2017.07.070

[29] Berrehal H, Makinde OD. Heat transfer analysis of CNTs-water nanofluid flow between nonparallel plates: Approximate solutions, Heat Transfer. 2021:1-15. DOI: https://doi.org/10.1002/htj.22112

[30] Ellahi R, Zeeshan A, Waheed A, Shehzad N, Sait SM. Natural convection nanofluid flow with heat transfer analysis of carbon nanotubes–water nanofluid inside a vertical truncated wavy cone. Mathematical Methods in the Applied Sciences. 2021:1-19. DOI: https://doi.org/10.1002/mma.7281

[31] Jayadevamurthy PGR, Rangaswamy NK, Prasannakumara BC, Nisar KS. Emphasis on unsteady dynamics of bioconvective hybrid nanofluid flow over an upward–downward moving rotating disk. Numerical Methods for Partial Differential Equations. 2020:1-22. DOI: 10.1002/num.22680

[32] Krishna MV, Chamkha AJ. Hall and ion slip effects on MHD rotating boundary layer flow of nanofluid past an infinite vertical plate embedded in a porous medium. Results in Physics. 2019:15:1-10. DOI: https://doi.org/10.1016/j.rinp.2019.102652

[33] Das S, Tarafdar B, Jana RN. Hall effects on unsteady MHD rotating flow past a periodically accelerated porous plate with slippage. European Journal of Mechanics / B Fluids. 2018:72:135-143. DOI: https://doi.org/10.1016/j.euromechflu.2018.04.010

[34] Krishna MV, Ahamad NA, Chamkha AJ. Hall and ion slip effects on unsteady MHD free convective rotating flow through a saturated porous medium over an exponential accelerated plate. Alexandria Engineering Journal. 2020:59(2):565-577. DOI: https://doi.org/10.1016/j.aej.2020.01.043

[35] Krishna MV, Ahamad NA, Chamkha AJ. Numerical investigation on unsteady MHD convective rotating flow past an infinite vertical moving porous surface, Ain Shams Engineering Journal. 2020:1-11. DOI: https://doi.org/10.1016/j.asej.2020.10.013

[36] Kumam P, Shah Z, Dawar A, Rasheed HU, Islam S. Entropy generation in MHD radiative flow of CNTs Casson nanofluid in rotating channels with heat source/sink, Mathematical Problems in Engineering. 2019:2019(9158093):1-14. DOI: https://doi.org/10.1155/2019/9158093

[37] Imtiaz M, Hayat T, Alsaedi A, Ahmad B. Convective flow of carbon nanotubes between rotating stretchable disks with thermal radiation effects. International Journal of Heat and Mass Transfer. 2016:101:948-957. DOI: http://dx.doi.org/10.1016/j.ijheatmasstransfer.2016.05.114

[38] Mosayebidorcheh S, Hatami M. Heat transfer analysis in carbon nanotube-water between rotating disks under thermal radiation conditions. Journal of Molecular Liquids. 2017:240:258-267. DOI: http://dx.doi.org/10.1016/j.molliq.2017.05.085

[39] Acharya N, Das K, Kundu PK. Rotating flow of carbon nanotube over a stretching surface in the presence of magnetic field: a comparative study. Applied Nanoscience. 2018:8(3):369-378. DOI: https://doi.org/10.1007/s13204-018-0794-9

[40] Mohamad AQ, Khan I, Ismail Z, Shafie S. Exact solutions for unsteady

free convection flow over an oscillating plate due to non-coaxial rotation. Springerplus. 2016:5(1):1-22. DOI: 10.1186/s40064-016-3748-2

[41] Mohamad AQ, Khan I, Shafie S, Isa ZM, Ismail Z. Non-coaxial rotating flow of viscous fluid with heat and mass transfer. Neural Computing and Applications. 2017:30(9):1-17. DOI: https://doi.org/10.1007/s00521-017-2854-6

[42] Mohamad AQ, Khan I, Jiann LY, Shafie S, Isa ZM, Ismail Z. Double convection of unsteady MHD non-coaxial rotation viscous fluid in a porous medium, Bulletin of the Malaysian Mathematical Sciences Society. 2018:41(4):2117-2139. DOI: https://doi.org/10.1007/s40840-018-0627-8

[43] Ersoy HV. Unsteady flow due to a disk executing non-torsional oscillation and a Newtonian fluid at infinity rotating about non-coaxial axes. Sādhanā. 2017:42(3):307-315. DOI: 10.1007/s12046-017-0600-5

[44] Mohamad AQ, Jiann LY, Khan I, Zin NAM, Shafie S, Ismail Z. Analytical solution for unsteady second grade fluid in presence of non-coaxial rotation. Journal of Physics: Conference Series. 2017:890(1):1-7. DOI: 10.1088/1742-6596/890/1/012040

[45] Mohamad AQ, Khan I, Zin NAM, Isa ZM, Shafie S, Ismail Z. Mixed convection flow on MHD non-coaxial rotation of second grade fluid in a porous medium, AIP Conference Proceedings. 2017:1830(1):020044. DOI: https://doi.org/10.1063/1.4980907

[46] Rafiq SH, Nawaz M, Mustahsan M. Casson fluid flow due to non-coaxial rotation of a porous disk and the fluid at infinity through a porous medium, Journal of Applied Mechanics and Technical Physics. 2018:59(4):601-607. DOI: 10.1134/S0021894418040053

[47] Rana S, Iqbal MZ, Nawaz M, Khan HZI, Alebraheem J, Elmoasry A. Influence of chemical reaction on heat and mass transfer in MHD radiative flow due to non-coaxial rotations of disk and fluid at infinity. Theoretical Foundations of Chemical Engineering. 2020:54(4):664-674. DOI: 10.1134/S0040579520040247

[48] Mohamad AQ, Ismail Z, Omar NFM, Qasim M, Zakaria MN, Shafie S, Jiann LY. Exact solutions on mixed convection flow of accelerated non-coaxial rotation of MHD viscous fluid with porosity effect, Defect and Diffusion Forum. 2020:399:26-37. DOI: 10.4028/www.scientific.net/DDF.399.26

[49] Noranuar WNN, Mohamad AQ, Shafie S, Khan I. Accelerated non-coaxial rotating flow of MHD viscous fluid with heat and mass transfer, IOP Conference Series: Materials Science and Engineering. 2021:1051(1):012044. DOI: 10.1088/1757-899X/1051/1/012044

[50] Das S, Tarafdar B, Jana RN. Hall effects on magnetohydrodynamics flow of nanofluids due to non-coaxial rotation of a porous disk and a fluid at infinity. Journal of Nanofluids. 2018:7(6):1172-1186. DOI: https://doi.org/10.1166/jon.2018.1527

[51] Ashlin TS, Mahanthesh B. Exact solution of non-coaxial rotating and non-linear convective flow of Cu–Al2O3–H2O hybrid nanofluids over an infinite vertical plate subjected to heat source and radiative heat. Journal of Nanofluids. 2019:8(4):781-794. DOI: https://doi.org/10.1166/jon.2019.1633

[52] Tiwari RK, Das MK. Heat transfer augmentation in a two-sided lid-driven differentially heated square cavity utilizing nanofluids. International Journal of Heat and Mass Transfer. 2007:50:2002-2018. DOI: https://doi.org/10.1016/j.ijheatmasstransfer.2006.09.034

[53] Stehfest H. Algorithm 368: Numerical inversion of Laplace transforms [D5]. Communications of the ACM. 1970:13(1):47-49. DOI: https://doi.org/10.1145/361953.361969

[54] Villinger H. Solving cylindrical geothermal problems using the Gaver-Stehfest inverse Laplace transform. Geophysics. 1985:50(10):1581-1587. DOI: https://doi.org/10.1190/1.1441848